

## CONVECTION DURING THE LATE STAGES OF SIMMERING IN TYPE IA SUPERNOVAE

ANTHONY L. PIRO AND PHILIP CHANG<sup>1</sup>

Astronomy Department and Theoretical Astrophysics Center, University of California, Berkeley, CA 94720;  
tpiro@astro.berkeley.edu, pchang@astro.berkeley.edu

*Accepted for publication in The Astrophysical Journal*

### ABSTRACT

Following unstable ignition of carbon, but prior to explosion, a white dwarf (WD) in a Type Ia supernova (SN Ia) undergoes a simmering phase. During this time, a central convective region grows and encompasses  $\sim 1M_{\odot}$  of the WD over a timescale of  $\sim 10^3$  yrs, which sets the thermal and turbulent profile for the subsequent explosion. We study this time-dependent convection and summarize some of the key features that differ from the traditional, steady-state case. We show that the long conductive timescale above the convective zone and the extraction of energy to heat the WD core leads to a decrease of the convective luminosity and characteristic velocities near the convective zone's top boundary. In addition, differences in the composition between the convective core and the conductive exterior will significantly alter the location of this boundary. In this respect, we find the biggest effect due to complete  $^{22}\text{Ne}$  sedimentation prior to carbon ignition. These effects add diversity to the possible WD models, which may alter the properties of the SN Ia explosion.

*Subject headings:* convection — supernovae: general — white dwarfs

### 1. INTRODUCTION

The use of Type Ia supernovae (SNe Ia) as cosmic distance indicators has focused attention to the study of white dwarf (WD) explosions. Of particular importance is determining the parameters that dictate the observed diversity of SNe Ia. Recent modeling demonstrates that the variation along the width-luminosity relation (Phillips et al. 1999) may be explained by large variations in the abundance of stable iron group elements (Kasen & Woosley 2007; Woosley et al. 2007) with the dominant cause for diversity likely residing in the explosion mechanism (Mazzali et al. 2007). Another important variable is the metallicity of the WD core (Timmes et al. 2003).

It is critical to explore the initial conditions that may add to the diversity. Simulations of turbulent thermonuclear flames in WDs have demonstrated that the composition and energy of ejecta depend sensitively on the competition between flame propagation, instabilities driven by turbulence, and expansion of the WD (Hillebrandt & Niemeyer 2000, and references therein). These simulations should therefore depend on the thermal and turbulent state of the WD set by the pre-explosive convective simmering phase (Nomoto et al. 1984; Woosley & Weaver 1986).

During the early stages of simmering many studies have focused on the convective Urca process (Paczynski 1972; Bruenn 1973; Couch & Arnett 1975; Iben 1978a,b, 1982; Barkat & Wheeler 1990; Mochkovitch 1996; Stein et al. 1999; Bisnovatyi-Kogan 2001; Lesaffre et al. 2005; Stein & Wheeler 2006). This occurs when nuclei repeatedly electron capture and beta decay as they are carried by convection back and forth across the electron capture threshold density (the “Urca shell”). Although the energy loss from this process is most likely not great enough to cause global cooling, it can still have a significant effect on the convective motions (Lesaffre et al. 2005). Once the central temperature has grown above  $\approx (5 - 6) \times 10^8$  K

(which corresponds to  $\sim 10^5$  s before the burning wave begins), there is no longer time for electron captures on  $^{23}\text{Na}$  (Piro & Bildsten 2007), and the convective Urca process will cease. During the last  $\sim 10^5$  s any compositional gradients are mixed homogeneously by subsequent convection.

An additional place where simmering is important is for understanding the conditions within the WD immediately prior to the explosion (García-Senz & Woosley 1995; Höflich & Stein 2002; Woosley et al. 2004; Wunsch & Woosley 2004). The properties of the temperature fluctuations present in the convection set the size and distribution of the ignition points, which are crucial for determining the success of the subsequent burning wave (see Röpke et al. 2006, and references therein). The interaction of convection with rotation sets the morphology of convective motions (Kuhlen et al. 2006) as well as the overall rotation profile of the WD (Piro 2008).

The last way simmering has gained attention is in its ability to enhance the neutron abundance in the WD core (Piro & Bildsten 2007; Chamulak et al. 2007). This happens primarily via the reaction chain  $^{12}\text{C}(p, \gamma)^{13}\text{N}(e^-, \nu_e)^{13}\text{C}$ , where the protons are leftover from  $^{12}\text{C}$  burning. Depending on the amount of carbon that is consumed before burning becomes dynamical, as well as the density at which it takes place, this neutronization enhancement could very well be large enough to mask any trend expected with metallicity in environments that have roughly sub-solar metallicity.

In this present work we focus on the general properties of the simmering convection, with the aim of identifying characteristics that may introduce diversity to the SN Ia progenitors. We begin in §2 by presenting the main features of our models. We illustrate how time-dependent convection in the simmering phase differs from the familiar case of steady-state convection. In this new picture, the convective flux decreases outside the central heating zone due to both the heating of new material as the convective region grows and the inability to transfer significant energy to the conductive exterior. In §3 we explore the location of the top of the convective zone. We point out that degeneracy effects enhance the response of the

<sup>1</sup> Miller Institute for Basic Research, University of California, Berkeley, CA 94720.

boundary location to changes in composition. We conclude with a summary of our results and a discussion of future work in §4.

## 2. LUMINOSITY AND CHARACTERISTIC VELOCITIES FOR EXPANDING CONVECTION

We begin by summarizing the main features of our simmering models. (For further details, the interested reader should refer to Woosley et al. 2004; Lesaffre et al. 2006; Piro & Bildsten 2007; Piro 2008.) Unstable ignition of  $^{12}\text{C}$  occurs when the heating from carbon fusion beats neutrino cooling. The central temperature then rises and a convective zone grows outward, eventually encompassing  $\sim 1M_\odot$  of the WD after  $\sim 10^3$  yrs. As the central temperature,  $T_c$ , increases, carbon burning becomes more vigorous and the heating timescale,  $t_h \equiv (d \ln T_c / dt)^{-1}$ , gets shorter. This timescale in general depends on the size of the region responding to the rising central temperature at the core.

Simmering ends and a burning wave commences once  $t_h \lesssim t_{\text{conv}}$ , where  $t_{\text{conv}}$  is eddy overturn timescale. At these late times, individual eddies may experience significant heating during their transit (García-Senz & Woosley 1995), so that the temperature profile is no longer an adiabat and the entire convective core does not respond to the increasing central temperature. (In contrast, we show below that during the majority of the time  $t_h$  depends on the heat capacity of the entire convective mass.) This makes it difficult to exactly calculate the *precise* moment when simmering ends. For this reason Lesaffre et al. (2006) explore  $t_{\text{conv}} = \alpha t_h$ , where  $\alpha \lesssim 1$  parameterizes this uncertainty. Since we are only roughly concerned with resolving the end of the simmering phase, we take  $t_{\text{conv}} \approx t_h \approx c_p T_c / \epsilon$ , where  $c_p$  is the specific heat capacity at constant pressure,  $\epsilon$  is the heating from carbon burning, and all these quantities are evaluated at the WD center. This estimates that simmering should end when  $t_h \approx 7$  s at a central temperature and density of  $T_c \approx 7.8 \times 10^8$  K and  $\rho_c \approx 2.6 \times 10^9$  g cm $^{-3}$ , which is roughly in agreement with the results presented by Woosley et al. (2004) using the Kepler stellar evolution code (Weaver et al. 1978).

We follow the simmering phase by calculating a series of hydrostatic WD models, each with a different central temperature, but at a fixed mass (see Piro & Bildsten 2007; Piro 2008). For simplicity we ignore the convective Urca process since our focus is on the last  $\sim 10^5$  s. The timescale for thermal conduction across the WD is  $t_{\text{th}} \equiv K_c / R^2 \sim 10^6$  yrs, where  $K_c$  is the conductivity and  $R$  is the radius, which is much longer the timescale over which heating is occurring. Therefore the convection efficiently mixes entropy and the convective region nearly follows an adiabat out from the WD center. Outside the convective zone, we assume the WD is isothermal with a temperature  $T_i$ .

### 2.1. Convective Luminosity

To understand how time-dependent convection is different than from that normally found in steady-state convection, we focus on the time-dependent entropy equation

$$c_p \frac{\partial T}{\partial t} = \epsilon - \frac{\partial L_c}{\partial M_r}, \quad (1)$$

where  $L_c$  is the convective luminosity. This equation omits the work required to expand the WD as the heating takes place, which is a significant amount of energy and thus requires

some discussion. For each convective model we compared the total change in WD binding energy to the total change in internal energy of the electrons (which are primarily degenerate and relativistic), including the ion-electron Coulomb interaction energy (according to Chabrier & Potekhin 1998). These two quantities are equal to the numerical accuracy of our integrations, which demonstrates that all of the work required to expand the WD comes from changes in the internal energy of the electrons. Thus, the entropy created from nuclear burning all goes into convective motions or the internal thermal energy, and we are justified in omitting the binding energy and electron internal energy terms from equation (1).

The temperature profile in the convective zone follows an adiabat with a power law index  $n \equiv (\partial \ln T / \partial \ln P)_{\text{ad}}$ . The time derivative of the temperature at a given pressure can be expressed as

$$\begin{aligned} \partial T / \partial t &= (P/P_c)^n \left[ \partial T_c / \partial t + T_c \ln(P/P_c) \partial n / \partial t \right] \\ &\approx (P/P_c)^n \partial T_c / \partial t, \end{aligned} \quad (2)$$

where  $P_c$  is the central pressure, and for simplicity we are assuming that it does not change appreciably in time. From this we see that the timescale for the temperature change *at any pressure* is set by the central temperature change

$$\frac{\partial \ln T}{\partial t} = \frac{\partial \ln T_c}{\partial t} \equiv \frac{1}{t_h}. \quad (3)$$

Therefore there is a well-defined, global heating timescale,  $t_h^2$ . To account for the changing central pressure in a more rigorous calculation, we must take partial derivatives at constant mass coordinate,  $M_r$ . This can be performed by inverting the empirically found  $M_c(T_i, T_c)$  relation presented in Piro (2008; or see eq. [11] below), where  $T_i$  is the nearly isothermal temperature of the non-convective, conductive region. The result is

$$T(T_c, M_r) = 0.83 T_c \left[ 1 - \left( \frac{\mu_e}{2} \right)^2 \frac{M_r}{1.48 M_\odot} \right], \quad (4)$$

where  $\mu_e$  is the mean molecular weight per electron. This can be used to find  $(d \ln T / dt)_{M_r} = d \ln T_c / dt$ , which confirms our conclusion that  $t_h$  is the same at any depth within the convective zone.

Multiplying equation (1) by  $dM_r = 4\pi r^2 \rho dr$  and integrating,

$$\int_0^{M_r} c_p \frac{\partial T}{\partial t} dM_r = \int_0^{M_r} \epsilon dM_r - L_c(M_r) + L_c(0). \quad (5)$$

We pull  $t_h$  outside of the left-hand integral to find

$$\int_0^{M_r} c_p T \frac{\partial \ln T}{\partial t} dM_r = \frac{1}{t_h} \int_0^{M_r} c_p T dM_r = \frac{E_{\text{th}}(M_r)}{t_h}, \quad (6)$$

where  $E_{\text{th}}(M_r)$  is the integrated thermal energy up to a mass coordinate  $M_r$ . We set  $L_c(0) = 0$  and define the nuclear luminosity as  $L_{\text{nuc}} = \int \epsilon dM_r$ , so that equation (5) becomes

$$\frac{E_{\text{th}}(M_r)}{t_h} = L_{\text{nuc}}(M_r) - L_c(M_r) \quad (7)$$

Equation (7) expresses that the nuclear luminosity must either go into thermal heating or convective motions, and it is

<sup>2</sup> Note that this timescale is different than the local timescale,  $c_p T_c / \epsilon$ , used above for estimating the end of simmering. This is because, with the exception of late times, the convective zone is well-coupled.

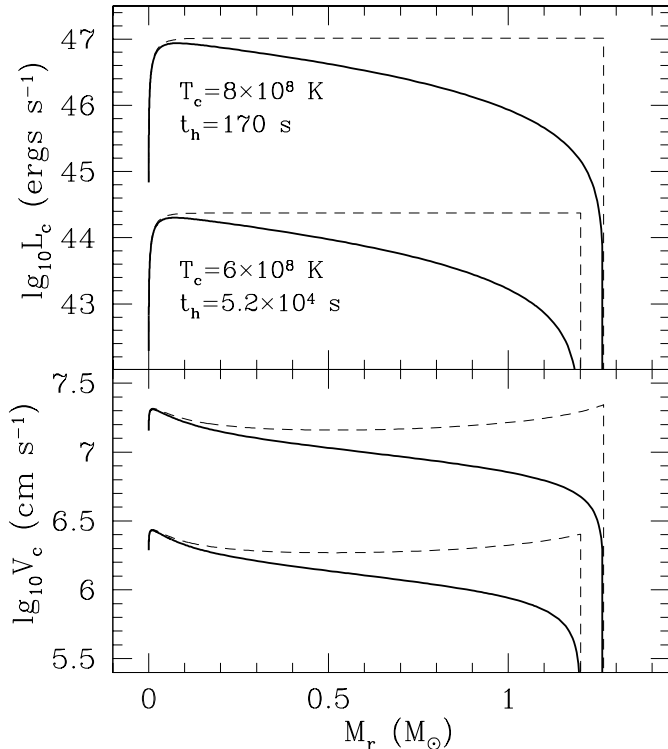


FIG. 1.— The convective luminosity,  $L_c$  and characteristic velocities,  $V_c$ , as a function of mass coordinate,  $M_r$ . The upper (lower) lines in each panel are for a central temperature of  $T_c = 8 \times 10^8$  K ( $6 \times 10^8$  K). Solid lines are the estimates for time-dependent convection using eq. (9). The dashed lines are calculations that assume  $L_c(M_r) = L_{\text{nuc}}(M_r)$ , which are plotted for comparison.

valid at any  $M_r$ . It contains two unknowns,  $t_h$  and  $L_c(M_r)$ . We set the luminosity at the surface of the convective zone to be zero,  $L_c(M_c) = 0$ . This boundary is required since  $t_{\text{th}}$  is long in the non-convective regions, which prevents significant heat transfer. We can then solve for  $t_h$ ,

$$t_h = E_{\text{th}}(M_c) / L_{\text{nuc}}(M_c), \quad (8)$$

which matches the definition of  $t_h$  that Weinberg et al. (2006) use in the context of type I X-ray bursts on neutron stars. We substitute  $t_h$  back into equation (7) to get the convective luminosity

$$\begin{aligned} L_c(M_r) &= L_{\text{nuc}}(M_r) - E_{\text{th}}(M_r) / t_h \\ &= L_{\text{nuc}}(M_r) \left[ 1 - \frac{E_{\text{th}}(M_r) L_{\text{nuc}}(M_c)}{E_{\text{th}}(M_c) L_{\text{nuc}}(M_r)} \right]. \end{aligned} \quad (9)$$

For steady-state convection,  $L_c(M_r) = L_{\text{nuc}}(M_r)$ . The ratio  $E_{\text{th}}(M_r) / E_{\text{th}}(M_c)$  is the modification due to the growing nature of the convection and the  $L_{\text{nuc}}(M_c) / L_{\text{nuc}}(M_r)$  term is from long thermal time for the conductive exterior, which forces  $L_c(M_c) = 0$ .

In the upper panel of Figure 1 we plot as solid lines the convective luminosity found using equation (9). These models all have a composition of 0.5  $^{12}\text{C}$ , 0.48  $^{16}\text{O}$ , and 0.02  $^{22}\text{Ne}$  by mass fraction, with a mass of  $1.37 M_{\odot}$  and an initial isothermal temperature  $T_i = 10^8$  K. We solve for  $\rho$  using the Paczyński (1983) fit for the equation of state, and include the Coulomb energy of Chabrier & Potekhin (1998). We present central temperatures of  $T_c = 6 \times 10^8$  and  $8 \times 10^8$  K, which corresponds to  $t_h = 14$  hrs and 170 s, respectively. The  $t_h$  associ-

ated with the latter case is an overestimate since, as mentioned above, at these late times during simmering only inner portion of the core responds to the rising central temperature (in effect decreasing  $E_{\text{th}}$  in eq. [8]). The energy generation rate for  $^{12}\text{C}$  burning is taken from Caughlan & Fowler (1988) with strong screening included from Salpeter & van Horn (1969). Also plotted in Figure 1 is the convective luminosity for  $L_c(M_r) = L_{\text{nuc}}(M_r)$ , i.e., for steady-state convection (dashed lines). Near the center,  $E_{\text{th}}(M_r)$  is small and grows less quickly than  $L_{\text{nuc}}(M_r)$ , so  $L_c(M_r)$  is initially  $\approx L_{\text{nuc}}(M_r)$  (see eq. [9]). At larger  $M_r$ ,  $L_c$  decreases due to the effects we have highlighted.

## 2.2. Convective Velocities

If we take a characteristic eddy scale  $l_c$ , the thermal conduction timescale across an eddy is  $\sim (l_c/R)^2 10^6$  yrs  $\sim (H/R)^2 10^6$  yrs  $\sim 10^4$  yrs, where  $H$  is the pressure scale height. Since this timescale is long, the convection is efficient (Hansen & Kawaler 1994). Using estimates from mixing-length theory, the characteristic convective velocity,  $V_{\text{conv}}$ , is related to  $F_{\text{conv}}$  via

$$V_c = \left( \frac{Q g l_c F_c}{c_p T \rho} \right)^{1/3} \sim \left( \frac{F_c}{\rho} \right)^{1/3}, \quad (10)$$

where  $Q = -(\partial \ln \rho / \partial \ln T)_P$  and  $g = GM_r / r^2$  is the local gravitational acceleration, and we have set  $l_c \approx H$ .

In the bottom panel of Figure 1 we have plotted  $V_c$ , setting the mixing-length to the scale height,  $l_c = H$  (solid lines). The shape of these velocity profiles are similar to those Lesaffre et al. (2005) present in the context of studying the convective Urca process, which is active at much earlier times during the simmering. The convective velocities are different by as much as  $\sim 50\%$  from the naïve estimate of  $L_c = L_{\text{nuc}}$  (dashed lines) near the top of the convective zone.

## 3. THE CONVECTIVE BOUNDARY LOCATION

Buoyantly rising eddies ascend until their density matches their surroundings. The boundary between the convective and isothermal zones is therefore set by a neutral buoyancy condition. In practice this means that both the pressure and density must be continuous. If both the convective and isothermal regions have the same composition, the boundary is simply set by when the adiabatic temperature of the convective zone reaches the isothermal temperature,  $T_i$  (i.e., where the entropy matches, Höflich & Stein 2002). If the composition is different, a buoyantly rising eddy will be prevented from passing very far into the isothermal region and truncates the size of the convective zone. This creates an abrupt change in temperature at the boundary of size  $\Delta T$ . In actuality this change will be smoothed by overshoot and mixing, so that the entropy remains continuous (see, for example, Kuhlen et al. 2006). The thermal and compositional structure at this boundary will be complicated, especially at the last moments of the simmering, when relatively few convective overturns take place for any given location of the convective boundary. Since the convection is always sub-sonic, we expect the overshoot to be modest and the simplification of a sharp compositional boundary to be adequate to estimate the size of the convective zone.

Piro (2008) presented an empirically derived relationship for the convective boundary,  $M_c$ , as a function of the ratio of

TABLE 1  
COMPOSITIONAL SUMMARY FOR NUMERICAL MODELS

Model	Purpose	Zone	$X_{12}$	$X_{13}$	$X_{16}$	$X_{22}$
1	Homogeneous	Convection	0.5	0.0	0.48	0.02
		Isothermal	0.5	0.0	0.48	0.02
2	Neutronization	Convection	0.48	0.02	0.48	0.02
		Isothermal	0.5	0.0	0.48	0.02
3	Comp. Gradient	Convection	0.5	0.0	0.5	0.0
		Isothermal	0.7	0.0	0.3	0.0
4	Sedimentation	Convection	0.487	0.0	0.487	0.026
		Isothermal	0.5	0.0	0.5	0.0

the isothermal and central temperatures,  $T_i/T_c$ ,

$$M_c = 1.48 M_\odot \left( \frac{2}{\mu_e} \right)^2 \left[ 1 - 1.2 \frac{T_i}{T_c} \right]. \quad (11)$$

We make the substitutions  $M_c \rightarrow M_c + \Delta M_c$  and  $T_i \rightarrow T_i + \Delta T$  to solve for the change in the convective mass due to a temperature discontinuity,

$$\Delta M_c = -0.18 M_\odot \left( \frac{2}{\mu_e} \right)^2 \left( \frac{8}{T_c/T_i} \right) \frac{\Delta T}{T_i}, \quad (12)$$

where we have scaled to a temperature ratio  $T_c/T_i = 8$ , as is appropriate for near the end of the simmering phase.

The temperature discontinuity allows a small conductive wave to propagate out from the top boundary of the convective zone. Since the thermal conduction timescale ( $t_{th} \sim 10^6$  yrs) is long in comparison to the heating timescale ( $t_h \sim 10$  s –  $10^3$  yrs), this wave can only travel a distance  $\sim (t_h/t_{th})^{1/2} H \ll H$  before the growing convective zone overtakes it. For this reason, we ignore this detail in the following calculations.

In the next sections we study the change in the convective boundary analytically. We discuss two main ways in which compositional discontinuities can be important. These are changes in the neutron abundance and changes in the composition, which affects the Coulomb corrections to the equation of state. In §3.3 we compare the models summarized in Table 1 numerically to confirm these analytic results.

### 3.1. Neutron Abundance Discontinuity

We first study differences in neutron abundance between the convective and isothermal zones. The neutronization is typically expressed as

$$Y_e = \frac{1}{\mu_e} = \sum_i \frac{Z_i}{A_i} X_i, \quad (13)$$

where  $A_i$  and  $Z_i$  are the nucleon number and charge of species  $i$  with mass fraction  $X_i$ . The initial metallicity of the SN Ia progenitor is determined by the isotope  $^{22}\text{Ne}$ , which has two additional neutrons (Timmes et al. 2003). A mass fraction  $X_{22}$  of  $^{22}\text{Ne}$  decreases  $Y_e$  by an amount  $\Delta Y_e = 2X_{22}/22 \approx 1.8 \times 10^{-3} X_{22}/0.02$ . A large enhancement of  $^{22}\text{Ne}$  could be present in the convective core if substantial gravitational separation has occurred (Bildsten & Hall 2001; Deloye & Bildsten 2002; García-Berro et al. 2007). Neutron enhancement in the convective zone can also occur from electron captures during the simmering, which decreases  $Y_e$  by an amount  $\Delta Y_e \sim 10^{-4} - 10^{-3}$  (Piro & Bildsten 2007; Chamulak et al. 2007).

We first consider the simplest equation of state where relativistic degenerate electrons dominate the pressure with corrections from the ideal gas of ions (in §3.2 we consider

Coulomb corrections),

$$P = K \left( \frac{\rho}{\mu_e} \right)^{4/3} + \frac{\rho k_B T}{\mu_e m_p}, \quad (14)$$

where  $K = 1.231 \times 10^{15}$  cgs and  $\mu_i$  is the mean molecular weight per ion.

We set the temperature to  $T_i + \Delta T$  and mean molecular weight per electron to  $\mu_e + \Delta \mu_e$  at the top of the convection zone, where  $T_i$  and  $\mu_e$  are the values of these quantities within the isothermal zone. We assume that  $\mu_i$  does not change appreciably. Note that enhanced neutronization in the convection implies  $\Delta \mu_e > 0$ . We set both  $P$  and  $\rho$  to be continuous at the convective boundary, and expand to first order,

$$\frac{\Delta T}{T_i} = \frac{4}{3} \frac{\mu_i m_p}{k_B T_i} K \frac{\rho^{1/3}}{\mu_e^{4/3}} \frac{\Delta \mu_e}{\mu_e}. \quad (15)$$

Recognizing that  $E_F = 4K(\rho/\mu_e)^{1/3} m_p$ , this can be written more conveniently as

$$\frac{\Delta T}{T_i} = \frac{1}{3} \frac{\mu_i}{\mu_e} \frac{E_F}{k_B T_i} \frac{\Delta \mu_e}{\mu_e} = \frac{1}{3} \frac{\mu_i}{\mu_e} \frac{E_F}{k_B T_i} \frac{\Delta Y_e}{Y_e}, \quad (16)$$

where we have defined  $\Delta Y_e$  to be positive (i.e.,  $\mu_e + \Delta \mu_e = Y_e - \Delta Y_e$ ). Setting  $E_F = 1.9 \text{ MeV} (2/\mu_e)^{1/3} \rho_8^{1/3}$ , where  $\rho_8 = \rho/10^8 \text{ g cm}^{-3}$ , this is rewritten as

$$\frac{\Delta T}{T_i} = 5.0 \times 10^2 \frac{\rho_8^{1/3}}{T_{i,8}} \left( \frac{\mu_i}{13.7} \right) \left( \frac{2}{\mu_e} \right)^{4/3} \frac{\Delta Y_e}{Y_e}, \quad (17)$$

where  $T_{i,8} = T_i/10^8 \text{ K}$  and  $\mu_i = 13.7$  for a plasma with  $X_{12} = X_{16} = 0.5$ . The large prefactor demonstrates that degeneracy greatly enhances the small changes in  $\mu_e$  on the temperature discontinuity. This is because the ions provide only a small contribution to the pressure, so that a large temperature jump is needed to offset a small change in density. Using equation (12), we find

$$\Delta M_c = -0.09 M_\odot \frac{\rho_8^{1/3}}{T_{c,8}/8} \left( \frac{\mu_i}{13.7} \right) \left( \frac{2}{\mu_e} \right)^{10/3} \frac{\Delta Y_e/Y_e}{10^{-3}}, \quad (18)$$

where  $T_{c,8} = T_c/10^8 \text{ K}$ . It is interesting to note that although  $T_i$  affects the absolute location of  $M_c$  (see eq. [11]),  $\Delta M_c$  is in fact *independent* of  $T_i$ .

### 3.2. Mean Molecular Weight per Ion and Coulomb Correction Discontinuities

We next consider the temperature difference from changes in the composition of the nuclei. This is of relevance because evolution of the progenitor star during the helium burning stage enhances  $^{12}\text{C}$  versus  $^{16}\text{O}$  with larger radii (Straniero et al. 2003).

First we present the effect of an increase of the mean molecular weight in the convection zone,  $\Delta \mu_i$ , using the equation of state given by equation (14). Setting the density and pressure continuous across the convective boundary,

$$\frac{\Delta T}{T_i} = \frac{\Delta \mu_i}{\mu_i}. \quad (19)$$

As a concrete example, we consider the composition in Model 3 from Table 1, which gives  $\Delta \mu_i/\mu_i \approx 0.06$ . This implies a

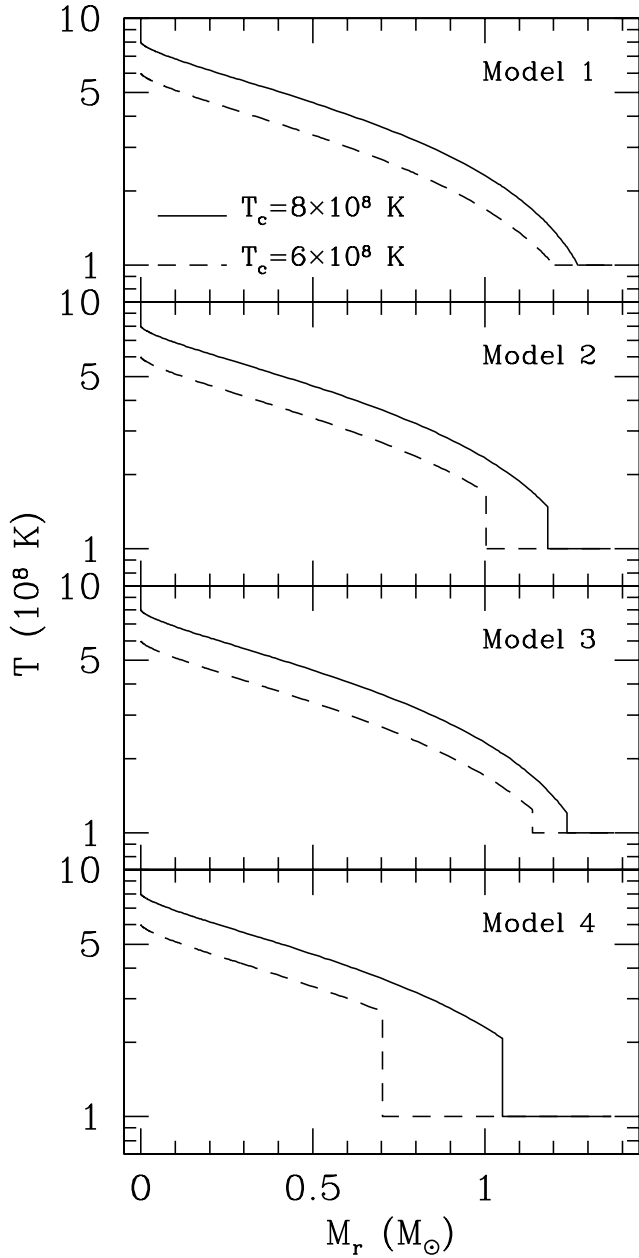


FIG. 2.— Temperature profiles for the compositional models summarized in Table 1. For each model we consider a central temperature of  $T_c = 6 \times 10^8$  K (dashed lines) and  $T_c = 8 \times 10^8$  K (solid lines). All models have an isothermal temperature of  $T_i = 10^8$  K and a mass of  $1.37 M_\odot$ . The convective boundary is at the temperature break.

change in convective mass of

$$\Delta M_c = -1.1 \times 10^{-2} M_\odot \frac{\rho_8^{1/3}}{T_{c,8}/8} \left( \frac{2}{\mu_e} \right)^2 \frac{\Delta \mu_i / \mu_i}{0.06}, \quad (20)$$

which is negligible.

However, compositional changes also alter the Coulomb contributions to the internal energy. For a multi-component plasma, the strength of this effect is measured via the Coulomb parameter

$$\Gamma = \frac{\langle Z^2 \rangle e^2}{ak_B T} = 21.1 \frac{\rho_8^{1/3} \langle Z^2 \rangle}{T_8} \left( \frac{13.7}{\mu_i} \right)^{1/3}, \quad (21)$$

(Schatz et al. 1999) where  $a$  is the mean ion separation defined as  $4\pi a^3 \rho / (3\mu_i m_p) = 1$  and

$$\langle Z^2 \rangle = \mu_i \sum_i \frac{Z_i^2}{A_i} X_i. \quad (22)$$

We take the fitting function found by Chabrier & Potekhin (1998) in the limit  $\Gamma \gg 1$  to model Coulomb effects,

$$P = K \left( \frac{\rho}{\mu_e} \right)^{4/3} + \frac{\rho k_B T}{\mu_i m_p} \left[ 1 - \frac{A_1}{3} \Gamma \right], \quad (23)$$

where  $A_1 = 0.9052$  is a fitting parameter. To isolate the compositional and temperature dependencies of  $\Gamma$ , we write  $\Gamma = \Gamma_0 / T$ . Within the convection,  $\Gamma$  is larger by a fractional amount

$$\frac{\Delta \Gamma}{\Gamma} = \frac{\Delta \Gamma_0}{\Gamma_0} - \frac{\Delta T}{T}, \quad (24)$$

where  $\Delta \Gamma_0$  is strictly from changes in composition (i.e., changes in  $\langle Z^2 \rangle$  and  $\mu_i$ ). Setting the pressure to be continuous across the convective boundary we find

$$\frac{\Delta T}{T_i} = \frac{A_1}{3} \Gamma \frac{\Delta \Gamma_0}{\Gamma_0}. \quad (25)$$

Due to the factor of  $\Gamma$ , a small fractional change  $\Delta \Gamma_0 / \Gamma_0$  of merely  $\sim 10\%$  (as present for Model 3) implies a mass change of

$$\Delta M_c = -0.12 M_\odot \frac{\rho_8^{1/3} \langle Z^2 \rangle}{T_{c,8}/8} \left( \frac{13.7}{\mu_i} \right)^{1/3} \left( \frac{2}{\mu_e} \right)^2 \frac{\Delta \Gamma_0 / \Gamma_0}{0.1}. \quad (26)$$

Comparing equations (18), (20), and (26) shows that both changes in  $Y_e$  and in Coulomb corrections can make non-negligible corrections to the convective boundary. Which effect is largest depends on the specific progenitor model.

### 3.3. Numerical Models

We now calculate a few models to compare how the convective boundary changes due to compositional discontinuities. These models use the same microphysics as described in §2.1. Each model is summarized in Table 1 and is motivated by a plausible progenitor scenario. Model 1 does not have a compositional discontinuity and is included for purposes of comparison. Model 2 shows the effects of neutronization by having a  $\Delta Y_e \approx 8 \times 10^{-4}$ , comparable to the level of neutronization found by Piro & Bildsten (2007). For simplicity we assume that all the additional neutrons are in  $^{13}\text{C}$  (instead of heavier elements such as  $^{23}\text{Ne}$ ). Model 3 considers a change in the mass fractions of  $^{12}\text{C}$  and  $^{16}\text{O}$  to show the effects of a compositional gradient. Finally, Model 4 shows the maximum effect of sedimentation by assuming that all of the  $^{22}\text{Ne}$  has sunk into the convective core.

In Figure 2 and 3 we compare the four models for central temperatures of  $T_c = 6 \times 10^8$  K and  $8 \times 10^8$  K, and a WD mass of  $1.37 M_\odot$ . In Figure 2 we set  $T_i = 10^8$  K, while in Figure 3 we set  $T_i = 2 \times 10^8$  K. While our models are not self-consistent in that we assume a fixed, non-evolving compositional discontinuity, they show that the location of the convective boundary can vary substantially depending on the progenitor model and the nuclear reactions that take place during the simmering. Comparing Figures 2 and 3 shows that  $\Delta M_c$  can be large

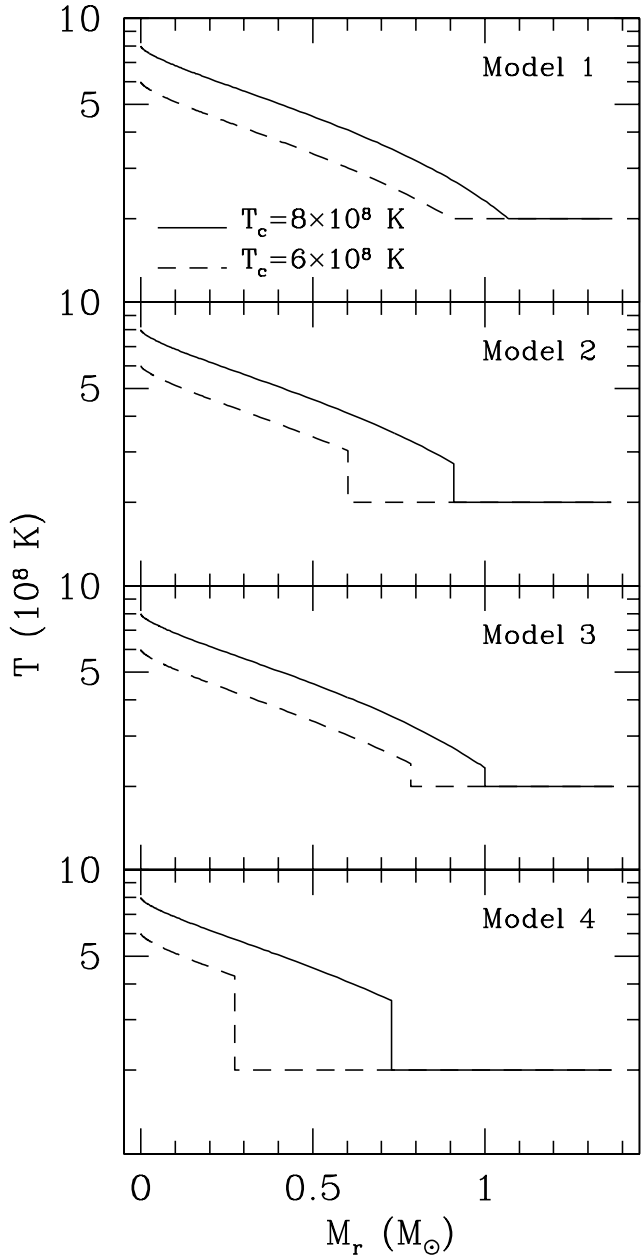


FIG. 3.— The same as Fig. 2, but with  $T_i = 2 \times 10^8$  K.

even when  $T_i$  is increased. This is roughly consistent with the analytics of §§3.1 and 3.2 that shows  $\Delta M_c$  is independent of  $T_i$ .

#### 4. CONCLUSION AND DISCUSSION

We have highlighted some important properties of the convection present during the pre-explosive carbon simmering phase of SNe Ia. The convective velocities near the top boundary are decreased significantly because the convective luminosity is extracted to heat and grow the convective zone and the long conductive timescale of the non-convective exterior enforces  $L_c = 0$  at the top of the convective zone. The size of the convective zone can change depending on compositional gradients within the progenitor WD.

Perhaps the most severe effect depends on whether there is

time available for sedimentation of  $^{22}\text{Ne}$  prior to carbon ignition. There remains considerable uncertainty in the timescale for this process to occur. For a  $1.2M_\odot$  WD, complete sedimentation requires  $\sim 9$  Gyr (Deloye & Bildsten 2002) with more massive WDs having an even shorter sedimentation time, but this all depends sensitively on the size of the diffusion coefficient used. The significant impact this may have on SNe Ia progenitors means that better theoretical calculations of this diffusion coefficient is an essential concern. The work by Daligault (2006) is an important step in this direction, but the multi-component plasma present in the WD may be a crucial detail.

The presence of the convective core prior to explosive carbon burning may have other implications for SNe Ia that deserve a closer look. The convective motions should give rise to a massive core dynamo, which setting  $B^2/8\pi \sim \rho V_c^2$  implies fields on the order of  $B \sim 10^{12}$  G. In addition, the motion of these convective eddies may stochastically excite waves (both  $g$ -modes and  $p$ -modes). These waves propagate away from the convective zone and transfer energy to shallower regions. Both of these processes may prove important in understanding the evolution toward explosive burning, and we plan to investigate them in more detail in a future study.

Multidimensional simulations are needed to study the physics of this simmering phase not captured by our simple calculation. These simulations are very challenging in that the flow must be followed for many turnover times. As a result, implicit Eulerian schemes (see for instance in two dimensions of Höflich & Stein 2002; Stein & Wheeler 2006), anelastic codes (Kuhlen et al. 2006) or a low Mach number formulation (Almgren et al. 2006a,b) are required. These simulations will be helpful in characterizing the flow topology (e.g., Kuhlen et al. 2006) and the number and spatial distribution of ignition points.

The simmering phase helps set the nature of the eventual runaway and subsequent explosion. Woosley et al. (2004) and Wunsch & Woosley (2004) demonstrate that the simmering is paramount for setting the initial ignition points for explosive burning. The large scale structure of the convective turbulence may also be important for flame propagation. For instance, Höflich & Stein (2002) argue that the initial velocities of the burning fronts are determined by the background convective motions and not by the laminar flame speed or Rayleigh-Taylor instabilities. This suggests that the initial explosive burning is likely to be off-centered (García-Senz & Woosley 1995; Woosley et al. 2004). The background turbulent state will also likely subsequently affect the motion of the bubbles by acting as a viscous drag (Zingale & Dursi 2007).

Finally, the material above the convective core is devoid of this turbulence. The burning properties may change in an interesting manner as the flame passes into this relatively "quiet" region. Some have argued that a delayed detonation transition (DDT) of the burning may be needed to match observations (Plewa et al. 2004; Livne et al. 2005). Although the concept of a DDT has been considered for some time (Khokhlov 1991; Woosley & Weaver 1994), how and if it occurs is still uncertain (Niemeyer & Woosley 1997; Niemeyer 1999; Woosley 2007). The position of the convective boundary may be an important detail. At the end of simmering it typically lies at a density of  $\sim 3 \times 10^7 - 10^8$  g cm $^{-3}$ , which may become near the density usually invoked for a DDT ( $\sim 10^7$  g cm $^{-3}$ ) once the WD has expanded from the propa-

gation of the deflagration wave.

and Stan Woosley for helpful discussions. P. C. is supported by the Miller Institute for Basic Research.

We thank Lars Bildsten, Eliot Quataert, Nevin Weinberg,

## REFERENCES

- Almgren, A. S., Bell, J. B., Rendleman, C. A., & Zingale, M. 2006a, *ApJ*, 637, 922
- Almgren, A. S., Bell, J. B., Rendleman, C. A., & Zingale, M. 2006b, *ApJ*, 649, 927
- Barkat, Z., & Wheeler, J. C. 1990, *ApJ*, 355, 602
- Bildsten, L. & Hall, D. M. 2001, *ApJ*, 549, L219
- Bisnovatyi-Kogan, G. S. 2001, *MNRAS*, 321, 315
- Bruenn S. 1973, *ApJ*, 183, L125
- Caughlan, G. R., & Fowler, W. A. 1988, *At. Data Nucl. Data Tables*, 40, 283
- Chabrier, G., & Potekhin, A. Y. 1998, *Phys. Rev. E*, 58, 4941
- Chamulak, D. A., Brown, E. F., Timmes, F. X., & Dupczak, K. 2007, submitted to *ApJ*
- Couch, R. G., & Arnett, W. D. 1975, *ApJ*, 196, 791
- Daligault J., 2006, *Phys. Rev. Lett.*, 96, 065003
- Deloye, C. J. & Bildsten, L. 2002, *ApJ*, 580, 1077
- García-Berro, E., Althaus, L. G., Córscico, A. H., & Isern, J. 2007, to appear in *ApJ* (arXiv:0712.1212)
- García-Senz, D. & Woosley, S. E. 1995, *ApJ*, 454, 895
- Hansen, C. J. & Kawaler, S. D. 1994, *Stellar Interiors: Physical Principles, Structure, and Evolution* (Berlin: Springer)
- Hillebrandt, W. & Niemeyer, J. C. 2000, *ARA&A*, 38, 191
- Höflich, P. & Stein, J. 2002, *ApJ*, 568, 779
- Iben, I. 1978a, *ApJ*, 219, 213
- Iben, I. 1978b, *ApJ*, 226, 996
- Iben, I. 1982, *ApJ*, 253, 248
- Kasen, D., & Woosley, S. E. 2007, *ApJ*, 656, 661
- Khokhlov, A. M. 1991, *A&A*, 245, 114
- Kuhlen, M., Woosley, S. E., & Glatzmaier, G. A. 2006, *ApJ*, 640, 407
- Lesaffre, P., Han, Z., Tout, C. A., Podsiadlowski, Ph., & Martin, R. G., 2006, *MNRAS*, 368, 187
- Lesaffre, P., Podsiadlowski, Ph., & Martin, C. A., 2005, *MNRAS*, 356, 131
- Livne, E., Asida, S. M., & Höflich, P. 2005, *ApJ*, 632, 443
- Mazzali, P. A., Roepke, F. K., Benetti, S. & Hillebrandt, W. 2007, *Science*, 315, 825
- Mochkovitch, R. 1996, *A&A*, 311, 152
- Niemeyer, J. C. 1999, *ApJ*, 523, L57
- Niemeyer, J. C., & Woosley, S. E. 1997, *ApJ*, 475, 740
- Nomoto, K., Thielemann, F.-K., & Yokoi, K. 1984, *ApJ*, 286, 644
- Paczynski, B. 1972, *Astrophys. Lett.*, 11, 53
- Paczynski, B. 1983, *ApJ*, 267, 315
- Phillips, M. M., Lira, P., Suntzeff, N. B., Schommer, R. A., Hamuy, M., & Maza, J. 1999, *AJ*, 118, 1766
- Piro, A. L. 2008, accepted for publication in *ApJ* (arXiv:0801.1107)
- Piro, A. L. & Bildsten, L. 2007, accepted for publication in *ApJ* (arXiv:0710.1600)
- Plewa, T., Calder, A. C., & Lamb, D. Q. 2004, *ApJ*, 612, L37
- Röpke, F. K., Hillebrandt, W., Niemeyer, J. C., & Woosley, S. E. 2006, *A&A*, 448, 1
- Salpeter, E. E., & van Horn, H. M. 1969, *ApJ*, 155, 183
- Schatz, H., Bildsten, L., Cumming, A. & Wiescher, M. 1999, *ApJ*, 524, 1014
- Stein, J., Barkat, Z., & Wheeler, J. C. 1999, *ApJ*, 523, 381
- Stein, J. & Wheeler, J. C. 2006, *ApJ*, 643, 1190
- Straniero, O., Domínguez, I., Imbriani, G., & Piersanti, L. 2003, *ApJ*, 583, 878
- Timmes, F. X., Brown, E. F., & Truran, J. W. 2003, *ApJ*, 590, L83
- Weaver, T. A., Woosley, S. E., & Zimmerman, G. B. 1978, *ApJ*, 225, 1021
- Weinberg, N. N., Bildsten, L., & Schatz, H. 2006, *ApJ*, 639, 1018
- Woosley, S. E. 2007, *ApJ*, 668, 1109
- Woosley, S. E., Kasen, D., Blinnikov, S., & Sorokina, E. 2007, *ApJ*, 662, 487
- Woosley, S. E., & Weaver, T. A. 1986, *ARA&A*, 24, 205
- Woosley, S. E., & Weaver, T. A. 1994, in *Les Houches Session LIV, Supernovae*, ed. S. Bludman, R. Mochovitch, & J. Zinn-Justin (Amsterdam: North Holland), 63
- Woosley, S. E., Wunsch, S., & Kuhlen, M. 2004, *ApJ*, 607, 921
- Wunsch, S. & Woosley, S. E. 2004, *ApJ*, 616, 1102
- Zingale, M. & Dursi, L. J. 2007, *ApJ*, 656, 333